AGU PUBLICATIONS

Global Biogeochemical Cycles

RESEARCH ARTICLE

10.1002/2014GB005079

Key Points:
- We assessed climate-carbon feedbacks with CESM1 to 2300 for RCP/ECP8.5
- Ocean carbon sensitivity to climate change proportional to heat content
- Climate influence on carbon largest in Atlantic Ocean and neotropical forests

Correspondence to:
J. T. Randerson,
jranders@uci.edu

Citation:
Randerson, J. T., K. Lindsay, E. Munoz, W. Fu, J. K. Moore, F. M. Hoffman, N. M. Mahowald, and S. C. Doney (2015), Multicentury changes in ocean and land contributions to the climate-carbon feedback, *Global Biogeochem. Cycles*, *29*, 744–759, doi:10.1002/2014GB005079.

Received 29 DEC 2014
Accepted 17 APR 2015
Accepted article online 21 APR 2015
Published online 2 JUN 2015

Multicentury changes in ocean and land contributions to the climate-carbon feedback

J. T. Randerson[1], K. Lindsay[2], E. Munoz[2], W. Fu[1], J. K. Moore[1], F. M. Hoffman[3], N. M. Mahowald[4], and S. C. Doney[5]

[1]Department of Earth System Science, University of California, Irvine, California, USA, [2]National Center for Atmospheric Research, Boulder, Colorado, USA, [3]Oak Ridge National Laboratory, Oak Ridge, Tennessee, USA, [4]Department of Earth and Atmospheric Sciences, Cornell University, Ithaca, New York, USA, [5]Woods Hole Oceanographic Institution, Woods Hole, Massachusetts, USA

Abstract Improved constraints on carbon cycle responses to climate change are needed to inform mitigation policy, yet our understanding of how these responses may evolve after 2100 remains highly uncertain. Using the Community Earth System Model (v1.0), we quantified climate-carbon feedbacks from 1850 to 2300 for the Representative Concentration Pathway 8.5 and its extension. In three simulations, land and ocean biogeochemical processes experienced the same trajectory of increasing atmospheric CO_2. Each simulation had a different degree of radiative coupling for CO_2 and other greenhouse gases and aerosols, enabling diagnosis of feedbacks. In a fully coupled simulation, global mean surface air temperature increased by 9.3 K from 1850 to 2300, with 4.4 K of this warming occurring after 2100. Excluding CO_2, warming from other greenhouse gases and aerosols was 1.6 K by 2300, near a 2 K target needed to avoid dangerous anthropogenic interference with the climate system. Ocean contributions to the climate-carbon feedback increased considerably over time and exceeded contributions from land after 2100. The sensitivity of ocean carbon to climate change was found to be proportional to changes in ocean heat content, as a consequence of this heat modifying transport pathways for anthropogenic CO_2 inflow and solubility of dissolved inorganic carbon. By 2300, climate change reduced cumulative ocean uptake by 330 Pg C, from 1410 Pg C to 1080 Pg C. Land fluxes similarly diverged over time, with climate change reducing stocks by 232 Pg C. Regional influence of climate change on carbon stocks was largest in the North Atlantic Ocean and tropical forests of South America. Our analysis suggests that after 2100, oceans may become as important as terrestrial ecosystems in regulating the magnitude of the climate-carbon feedback.

1. Introduction

Information about future climate scenarios needed by policy makers for climate adaptation and mitigation decisions often has contrasting time scales. Many adaptation efforts focus on expected changes over a period of the next several decades, commensurate with time scales for infrastructure planning, investment, and turnover. Through the middle of the 21st century, divergence among future climate scenarios is minimal and difficult to detect robustly given natural climate variability [*Tebaldi and Friedlingstein*, 2013]; much of the warming has been determined by past emissions and the response of the Earth system to this forcing [*Hansen et al.*, 2005]. For the design of mitigation policy, in contrast, climate information on longer time scales becomes increasingly relevant as the cumulative amount of emissions and warming [*Gillett et al.*, 2013] influences the magnitude of risk for biodiversity, ecosystem services, and human well-being [*Field et al.*, 2014]. Feedbacks between the climate system and the global carbon cycle also are expected to intensify on longer time scales, making it increasingly difficult to stabilize atmospheric CO_2 levels during the latter part of the 21st century [*Ciais et al.*, 2013; *Jones et al.*, 2013]. These feedbacks further contribute to the irreversibility of climate change, whereby warming, ice sheet melt, sea level rise, and drought effects persist for many centuries after the abatement of emissions [*Solomon et al.*, 2009; *Froelicher and Joos*, 2010; *Boucher et al.*, 2012; *Collins et al.*, 2013].

Recent analysis of climate-carbon feedbacks in Earth system models (ESMs) from the Fifth Phase of the Coupled Model Intercomparison Project (CMIP5) has primarily focused on idealized model simulations in which CO_2 levels increase at a rate of 1%/yr, starting from preindustrial levels and ending after CO_2 quadruples at approximately 1140 ppm. This work has provided important insight about the mechanisms

regulating carbon cycle feedbacks on decadal time scales and shows that mean sensitivity of carbon stocks in the ocean to warming is several fold lower than same sensitivity for the land [*Arora et al.*, 2013; *Ciais et al.*, 2013]. Within the ocean, temperature-driven decreases in solubility and changes in ocean transport and mixing (i.e., increased density stratification and reduced meridional overturning circulation) are primary mechanisms contributing to this sensitivity [*Schwinger et al.*, 2014]. On land, important processes regulating the climate sensitivity of carbon stocks in the current generation of ESMs include reductions in tropical net primary production in response to warming and drying [*Friedlingstein et al.*, 2006] and increases in decomposition of soil organic matter [*Friedlingstein et al.*, 2006; *Todd-Brown et al.*, 2014]. Losses from tropical ecosystems are partially offset in many models by longer growing seasons (and thus enhanced productivity) in boreal and tundra biomes. Detailed representation of permafrost processes was not included in models contributing to CMIP5, likely influencing the sign and magnitude of high-latitude terrestrial ecosystem contributions to the climate-carbon feedback. Similarly, these models generally do not include detailed, dynamic representations of the marine iron and nitrogen cycles [*Bopp et al.*, 2013], which influence carbon-climate feedbacks in the ocean. In the context of comparing different simulations, the diagnosis of feedback parameters has been shown to be scenario dependent and sensitive to the types of coupling experiments used to derive feedback parameters [*Gregory et al.*, 2009; *Zickfeld et al.*, 2011; *Schwinger et al.*, 2014].

Beyond 2100, the evolution of the carbon cycle and climate system has been investigated primarily using Earth system models of intermediate complexity [*Plattner et al.*, 2008; *Zickfeld et al.*, 2013]. On these longer time scales, much less work has been done to investigate climate-carbon cycle interactions using fully coupled ESMs, although several studies have employed ESMs to study the reversibility of biogeochemical and climate-related changes from CO_2 emissions [*Froelicher and Joos*, 2010; *Boucher et al.*, 2012]. Improving estimates of how carbon cycle dynamics are likely to change century by century for different Representative Concentration Pathway (RCP) scenarios is important for several reasons. First, it may enable us to identify low probability but high-risk events for marine and terrestrial ecosystems that inform the design of mitigation policy. Examples of such events may include reorganization (or shutdown) of ocean circulation patterns that influence future rates of carbon uptake [*Zickfeld et al.*, 2008] and the functioning of marine ecosystems [*Kuhlbrodt et al.*, 2009]. Fully coupled Earth system models are particularly well suited for this challenge because they often include a rigorous representation of ocean physics and ocean-atmospheric coupling. On land, the sustained impact of climate change on forests may be amplified over several generations, although the representation of mortality, recruitment, and competition processes are only beginning to be integrated within Intergovernmental Panel on Climate Change (IPCC)-class ESMs. One prominent example of a climate-carbon cycle feedback triggering an extreme event during the latter half of the 21st century is the Amazon dieback simulated within an early version of the Hadley model [*Betts et al.*, 2004]. Although a recent, emergent constraint analysis provides evidence that likelihood of such an event may be lower than earlier estimates [*Cox et al.*, 2013; *Wenzel et al.*, 2014], many lines of evidence indicate that this region remains vulnerable to interactions between changing temperature, drought stress, and land use [*Davidson et al.*, 2012]. In permafrost regions, time delays between soil heating and active layer thickening may cause carbon losses to accelerate considerably after 2100 [*Koven et al.*, 2015]. Second, information about climate-carbon feedbacks after 2100 can provide insight about whether a greenhouse gas stabilization scenario can be maintained over a period of centuries and whether more (or less) emission adjustments would be needed to remain below a desired threshold, including more intensive CO_2 emission abatement trajectories needed to avoid dangerous interference with the climate system [e.g., *Hansen et al.*, 2013].

Here we used the Community Earth System Model [*Hurrell et al.*, 2013] to investigate the century by century evolution of climate-carbon feedbacks from 1850 to 2300. We conducted three simulations in which we forced the model with the same atmospheric CO_2 mole fraction trajectory from historical Representative Concentration Pathway 8.5 (RCP8.5) and Extended Concentration Pathway 8.5 (ECP8.5) time series [*Meinshausen et al.*, 2011]. In one simulation changing CO_2 and all other greenhouse gases and aerosols influenced radiative transfer, in a second forcing from CO_2 was excluded, and in a third forcing from all greenhouse gases and aerosols was excluded. The simulations allowed us to quantify feedback parameters and to assess how the carbon cycle responded separately to climate change from CO_2 and from all anthropogenic atmospheric forcing agents. The large magnitude of atmospheric CO_2 increase in ECP8.5

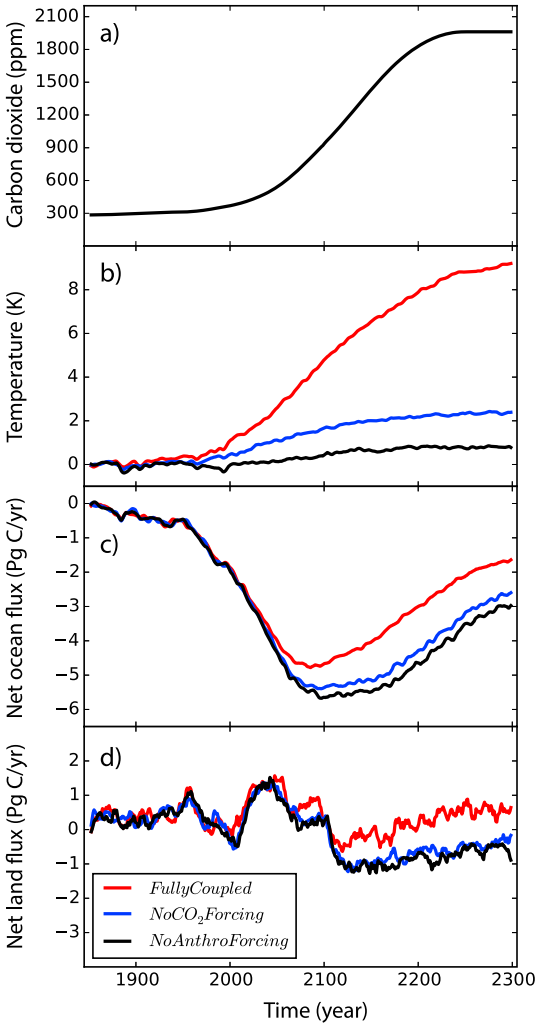

Figure 1. (a) Prescribed atmospheric carbon dioxide mole fractions for RCP8.5 and its extension and CESM1(BGC) estimates of (b) global mean surface air temperature change, (c) net ocean carbon flux, and (d) net land carbon flux. For the net carbon fluxes shown in Figures 1c and 1d, a positive flux denotes a release of carbon dioxide into the atmosphere from the ocean or land surface. Figures 1c and 1d have the same *y* axis scale. The red lines denote the fully coupled simulation, the blue lines denote the no CO_2 forcing simulation, and the black lines denote the no anthropogenic forcing simulation. A 5 year center-mean smoothing was applied to all of the variables in Figures 1b–1d.

(stabilizing at 1962 ppm), experimental design, and time span of our analysis (to 2300) set this study apart from past work investigating carbon cycle feedbacks. We show that both land and ocean carbon inventories have an increasing sensitivity to climate change after 2100 and that reductions in ocean carbon uptake increase considerably over time, making the ocean the primary contributor to the climate-carbon feedback during the 22nd and 23rd centuries.

2. Methods

We used the Community Earth System Model version 1.0 with biogeochemistry enabled [*Lindsay et al.*, 2014]. Interactive components with carbon cycling included the Community Atmosphere Model version 4 [*Neale et al.*, 2013], the Community Land Model version 4 (CLM4) [*D. M. Lawrence et al.*, 2012], and the Biogeochemical Elemental Cycling module [*Moore et al.*, 2013] that runs within the ocean physics model [*Gent et al.*, 2011; *Danabasoglu et al.*, 2012]. Spin-up of the carbon cycle using the Community Earth System Model version 1.0 with biogeochemistry enabled, hereafter referred to as CESM1(BGC), involved several different stages of partial coupling, including simulations between the land and a fixed preindustrial atmospheric CO_2 mole fraction, the ocean and a fixed atmospheric CO_2 mole fraction, and a subsequent interactive ocean-land-atmosphere simulation in which the atmospheric model allowed CO_2 to evolve as a three-dimensional tracer [*Lindsay et al.*, 2014]. Spin-up was followed by a 1000 year control simulation, with the experiments described below branching in the year 151. This year was the same as the one used for branching to the historical forcing in earlier CESM1(BGC) simulations delivered to the Coupled Model Intercomparison Project Phase 5 model archive on the Earth System Grid. Transient land cover change and wood harvesting were implemented within the plant functional type framework of CLM4 from 1850 to 2100 [*P. J. Lawrence et al.*, 2012] using land cover information derived from observations and future model scenarios [*Hurtt et al.*, 2011]. Evaluation of the performance of CESM1 (BGC) is described in detail by *Keppel-Aleks et al.* [2013] for atmospheric CO_2, by *Long et al.* [2013] for ocean carbon and chlorofluorocarbon observations, by *Moore et al.* [2013] for ecosystem dynamics and nutrient cycling, and by *Lindsay et al.* [2014] for responses to El Niño–Southern Oscillation and other dynamics.

We conducted three simulations with CESM1(BGC), in which atmospheric CO_2 followed the same prescribed time series. The CO_2 time series consisted of three fused segments corresponding to historical, RCP8.5 and ECP8.5 mole fractions. CO_2 mole fractions increased from approximately 285 ppm in 1850 to 1962 ppm in 2300 (Figure 1a). In all three simulations, biogeochemical processes in the ocean and on land responded

to the prescribed CO_2 time series (i.e., biogeochemical interactions were enabled). In one simulation, hereafter referred to as "fully coupled," all of the anthropogenic atmospheric forcing terms also were radiatively coupled. The forcing agents were CO_2, CH_4, chloroflourocarbons, ozone, aerosols, and aerosol deposition on snow. In a second simulation, hereafter referred to as "no CO_2 forcing," all of the conditions were identical to the fully coupled simulation, with the exception that for radiative transfer in the atmospheric model, CO_2 mole fractions were held at preindustrial (1850) levels. In a third simulation, hereafter referred to as "no anthropogenic forcing," all of the anthropogenic atmospheric forcing agents were held at 1850 levels. By comparing the fully coupled and no CO_2 forcing simulations, we were able to quantify how carbon feedback parameters changed over time and the impact of CO_2-induced climate change on compatible emissions. A similar comparison of fully coupled and no anthropogenic forcing simulations allowed us to assess the full impact of climate change on carbon cycle processes and compatible fossil fuel emissions. The difference between the no CO_2 forcing and no anthropogenic forcing simulations provided information about the impact of non-CO_2 greenhouse gases and aerosols on the carbon cycle.

In all three simulations, cropland area wood harvesting followed the same historical and RCP8.5 time series [*P. J. Lawrence et al.*, 2012]. After 2100 cropland areas were held constant and wood harvest rates were maintained at year 2100 levels. Similarly, land and ocean reactive nitrogen deposition followed the same spatially variable time series in all three simulations from 1850 to 2100 [*Lamarque et al.*, 2010] and thereafter were then held constant using maps from 2100. Plant functional type composition was prescribed at each grid cell and modified as a function of changing cropland area; other vegetation dynamics such as the movement of biomes from climate change were not simulated in this version of the model.

In our analysis we computed the gain, g, of the climate-carbon feedback using differences in cumulative compatible fossil fuel emissions between the fully coupled, E_{coupled}, and no CO_2 forcing, $E_{\text{no CO2}}$, simulations for different time intervals following equation (13) from *Arora et al.* [2013]:

$$g = \left(E_{\text{no CO2}} - E_{\text{coupled}}\right)/E_{\text{no CO2}} \tag{1}$$

We also used the integrated flux-based feedback parameters from *Arora et al.* [2013] to understand the drivers of the changing gain. In this context, γ_O and γ_L represent the sensitivity of cumulative ocean and land carbon fluxes to changes in global mean surface air temperature (with units of Pg C K^{-1}) and β_O and β_L represent the sensitivity of cumulative ocean and land carbon fluxes to changes in atmospheric carbon dioxide (with units of Pg C ppm^{-1}). A final parameter, α, represents the sensitivity of global mean surface air temperature to cumulative changes in atmospheric CO_2 (with units of K ppm^{-1}). Following from *Friedlingstein et al.* [2006] and *Arora et al.* [2013], g can be related to these feedback parameters through the following equation, after imposing several simplifying assumptions:

$$g = \alpha(\gamma_O + \gamma_L)/(m + \beta_O + \beta_L) \tag{2}$$

where m is a constant ($2.12\ \text{Pg C ppm}^{-1}$) and γ_O, γ_L, β_O, and β_L are defined above. We note that β_L diagnosed from the simulations used here includes the influence of land use change and thus cannot be directly compared with earlier estimates from *Arora et al.* [2013] or *Friedlingstein et al.* [2006] derived from more idealized simulations.

3. Results

3.1. Temperature and Carbon Cycle Responses

Global mean surface air temperature increased by 9.3 K from 1850 to 2300, with 4.4 K of this warming occurring after 2100 in the fully coupled model simulation (Figure 1b and Table 1). Without radiative forcing from CO_2, temperature increases were much smaller, reaching 2.4 K at 2300. From the difference between these two simulations, we estimated that warming induced solely by CO_2 interactions with the Earth's radiation budget was 6.9 K. In the absence of any atmospheric anthropogenic radiative forcing, some residual warming occurred (0.8 K) from the combined effects of changes in stomatal conductance and leaf area in response to elevated levels of atmospheric CO_2 and land use. The difference between

Table 1. Cumulative Carbon and Temperature Change From 1850

	Time (Year)			
Model State Variable	1999	2099	2199	2300
Atmospheric CO_2 (ppm)[a]	370	940	1831	1962
Temperature change, fully coupled (K)	1.18	4.88	7.98	9.27
Temperature change, no CO_2 forcing (K)	0.50	1.71	2.19	2.41
Temperature change, no anthropogenic forcing (K)	−0.03	0.43	0.74	0.76
Compatible fossil emissions, fully coupled (Pg C)	220	1721	4014	4455
Compatible fossil emissions, no CO_2 forcing (Pg C)	223	1781	4250	4900
Compatible fossil emissions, no anthropogenic forcing (Pg C)	229	1805	4317	5018
Ocean cumulative uptake, fully coupled (Pg C)	97	475	866	1080
Ocean cumulative uptake, no CO_2 forcing (Pg C)	98	507	1007	1332
Ocean cumulative uptake, no anthropogenic forcing (Pg C)	100	519	1051	1410
Land cumulative uptake, fully coupled (Pg C)	−57	−142	−129	−178
Land cumulative uptake, no CO_2 forcing (Pg C)	−55	−115	−34	15
Land cumulative uptake, no anthropogenic forcing (Pg C)	−51	−103	−12	54

[a]Atmospheric CO_2 levels at the beginning of the simulation in 1850 were 285 ppm; all other quantities were, by definition, zero.

the latter two simulations (1.6 K) described the influence of non-CO_2 greenhouse gases and aerosols for this scenario.

In response to climate change, ocean and land rates of carbon uptake were reduced, with the size of the impact increasing over time. In the oceans, the three trajectories noticeably diverged in the second half of the 21st century, with the maximum rate of ocean uptake in the fully coupled simulation reduced by 15% and occurring more than a decade earlier than in the no anthropogenic forcing simulation (Figure 1c). Land exchange was more variable on decadal time scales, with the net flux from the fully coupled simulation more positive than in the other two simulations for several multiyear periods during the 21st century and then continuously after the first decade of the 21st century (Figure 1d).

Reductions in cumulative ocean carbon uptake from anthropogenic climate change increased from 3% in 2005 to 23% in 2300 (Figure 2a and Table 1). By end of the simulation, this corresponded to a 330 Pg C reduction in the ocean carbon inventory. On land, the influence of climate change on the inventory also increased with time, causing a cumulative reduction of 232 Pg C (Figure 2b). Combining information from the ocean and land inventories, we found that climate change reduced compatible fossil fuel emissions for the scenario by 11%, from 5018 Pg C to 4455 Pg C (Table 1). Approximately half of the total climate-induced reduction in compatible emissions occurred during the final century of the simulation, during a period of rapid and sustained emission reductions required to allow atmospheric CO_2 to stabilize.

The transient climate response to cumulative carbon emissions (TCRE) has been used by IPCC Fifth Assessment [*Collins et al.*, 2013] as a means to compare different scenarios because of the path independence of final surface air temperature changes to cumulative fossil fuel emissions [*Matthews et al.*, 2009]. For the simulations analyzed here, TCRE was 3.1 through 1999, 1.84 through 2099, 1.44 through 2199, and 1.54K/1000 Pg C through 2300 as computed using compatible fossil fuel emissions from the fully coupled simulation and the global mean surface air temperature difference between the fully coupled and no CO_2 forcing simulations (Figure 3 and Table 1). When using the temperature difference from the fully coupled and no anthropogenic forcing simulations, the TCRE increased to 2.59 K/1000 Pg C at 2099, solely as a consequence of warming from non-CO_2 greenhouse gases and aerosols. This 40% increase from non-CO_2 forcing was considerably higher than the equivalent 15% boost given to the TCRE by *Friedlingstein et al.* [2014] for the same purpose in a study of emission scenarios needed to limit warming below 2 K. One likely explanation for the larger influence of non-CO_2 forcing agents observed here is the rapid buildup of N_2O and CH_4 in the RCP8.5 scenario, compared to smaller increases for these gases in RCP2.6 and other similar low-emission scenarios.

Over time, changes in the TCRE were considerable and can be inferred from changes in the slope in Figure 3. The strong concave down part of the curve between 1000 Pg C and 3000 Pg C of cumulative emissions corresponded to the interval between 2060 and 2140. During this period, the atmospheric CO_2 growth

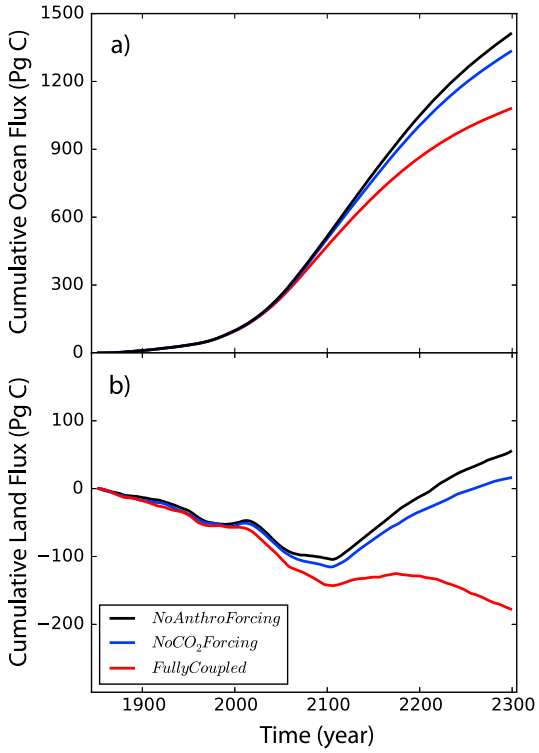

Figure 2. Cumulative uptake of carbon by (a) ocean and (b) land starting from 1850. Positive quantities denote carbon accumulation within the ocean or land reservoir.

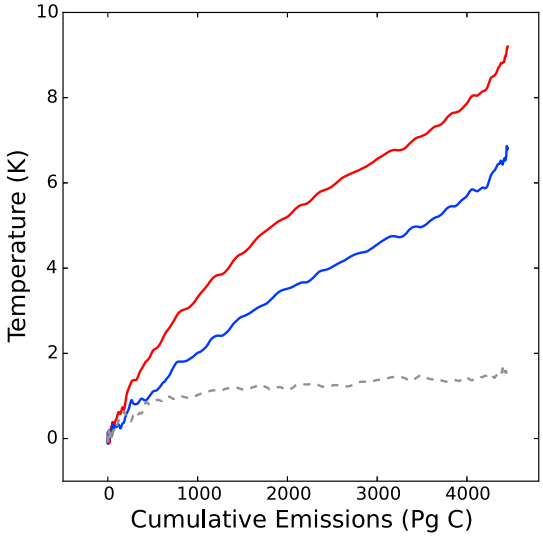

Figure 3. Global mean surface air temperature as a function of cumulative fossil fuel carbon emissions. Temperature change for the fully coupled simulation is shown in red, the difference between the fully coupled and the no CO_2 forcing simulation is shown in blue, and the difference between the no CO_2 and no anthropogenic forcing simulations is shown in gray. In all cases, compatible emissions from the fully coupled simulation are used here to estimate the transient climate response to cumulative emissions (TCRE).

rate was at its highest level in the simulation (Figure 1). Although the high rates of fossil emissions increased the airborne fraction (and thus atmospheric CO_2 available to drive warming), saturating radiative forcing at higher CO_2 mole fractions and high levels of ocean heat uptake more than compensated, leading to proportionally lower global mean surface air temperature changes. In contrast, during the final stage of the simulation (from 2200 to 2300) when steep cuts in compatible emissions were required to stabilize atmospheric CO_2, the temperature response was convex upward. The increasing TCRE during this latter period was likely a consequence of very low emissions, yet continued adjustments in temperature as the Earth system reestablished radiative equilibrium [e.g., *Hansen et al.*, 2005].

3.2. Climate-Carbon and Concentration-Carbon Feedback Parameters

The gain of the climate-carbon feedback (equation (1)) increased century by century, from 0.034 by 2100 to 0.091 by 2300 when estimated using the fully coupled and no CO_2 forcing simulations. The primary drivers of the increasing gain varied over time (Table 2). From 2100 to 2200, a 65% increase in the gain was consequence of several competing processes. Over this span, the sensitivity of ocean carbon uptake to temperature (γ_O) increased by a factor of 2.4, from $-10.1\,\mathrm{Pg\,C\,K^{-1}}$ to $-24.4\,\mathrm{Pg\,C\,K^{-1}}$ (Table 2). The sensitivity of land carbon uptake to temperature (γ_L) also increased but by a lesser degree. In parallel, the ocean became progressively less efficient at taking up carbon in response to atmospheric CO_2 increases, with β_O decreasing from $0.77\,\mathrm{Pg\,C\,ppm^{-1}}$ at 2100 to $0.65\,\mathrm{Pg\,C\,ppm^{-1}}$ at 2200. The decrease in β_O was likely caused by reduced ocean buffering capacity in response to higher pCO_2 levels, and concurrently, the coupling between the mixed layer and intermediate water masses becoming an increasingly important barrier limiting carbon flow in response to the increasing atmospheric CO_2 growth rate (Figure 1a). On land, it was likely that in unmanaged systems the efficacy of carbon accumulation per unit of atmospheric CO_2 also declined, but it was not possible to separate the influence of atmospheric CO_2 and land use change on β_L with our experimental design. Isolating the contribution of atmospheric CO_2 to β_L, and understanding how land use modifies β_L, requires additional model

Table 2. Climate-Carbon Feedback Parameters

	Time Period			
Parameter	1850–1999	1850–2100	1850–2200	1850–2300
α (K ppm^{-1})	0.0080	0.0048	0.0037	0.0041
β_O (Pg C ppm^{-1})	1.15	0.77	0.65	0.79
β_L (Pg C ppm^{-1})[a]	−0.65	−0.18	−0.02	0.01
γ_O (Pg C K^{-1})	−1.5	−10.1	−24.4	−36.7
γ_L (Pg C K^{-1})	−2.9	−8.5	−16.4	−28.1
Gain[b]	0.013	0.034	0.056	0.091

[a]Parameter β_L estimated from these simulations includes the influence of land use change in addition to biosphere responses to atmospheric CO_2 fertilization. As a result, this parameter cannot be directly compared with earlier estimates that only include the latter influence.
[b]Gain is estimated from compatible fossil emissions following equation (13) from *Arora et al.* [2013] from the difference between the fully coupled and no CO_2 forcing simulations. All other parameters in the table also were computed using cumulative carbon cycle quantities from these two simulations.

simulations and will not be further analyzed here. Positive drivers of the increasing gain from 2100 to 2200 were offset by reductions in the sensitivity of temperature to atmospheric CO_2 (α), which decreased from 0.0048 K ppm^{-1} to 0.0037 K ppm^{-1}. The reductions in α were likely a consequence of (1) the influence of CO_2 on radiative transfer becoming saturated at higher atmospheric concentrations [*Myhre et al.*, 1998] and (2) progressively more rapid rates of CO_2 rise that limited the magnitude of the temperature change for a given amount of added radiative forcing [*Collins et al.*, 2013]. This latter effect is consistent with past work indicating that the transient climate response is often considerably lower than the equilibrium climate response, as a consequence of the ocean having less time to adjust and warm to the same atmospheric CO_2 increment [*Hansen et al.*, 2005].

During the 23rd century, the gain further increased by another 64% as a consequence of different driving processes. During this period, atmospheric CO_2 rose much more slowly in the RCP/ECP8.5 scenario (by 7.8%) as the atmospheric mole fraction approached steady state at 1962 ppm. The change in global mean surface air temperature (1.3 K) was proportionally larger than the change in CO_2 because Earth system components that responded more slowly to radiative forcing continued to adjust. Model components that required longer equilibration times included deeper ocean layers that once modified, slowly increased warming at the surface. As a consequence, compared to the 22nd century, α increased by 9%. The added warming interacted with significant increases in the climate sensitivity of both ocean and land net carbon fluxes (γ_O and γ_L) as positive drivers of the gain. These drivers were counterbalanced by increases in β_O and β_L. Analogous to the mechanism driving up α, slower increases in atmospheric CO_2 reduced the impact of bottlenecks of anthropogenic carbon inflow associated with coupling between surface and intermediate waters in the ocean and on land enabled more stabilization of carbon in longer-lived wood, litter, and soil organic carbon pools for the same atmospheric CO_2 increment [*Gregory et al.*, 2009]. This effect—that the efficacy of carbon uptake by land and ocean reservoirs increases with a more gradual trajectory of atmospheric CO_2 rise—is consistent with earlier work indicating that the atmospheric CO_2 airborne fraction is primarily regulated by the growth rate of fossil fuel emissions [*Gloor et al.*, 2010].

To further assess the drivers of the increasing gain from 2100 to 2300, we isolated the contribution of changing individual parameters using equation (2). First, we confirmed that equation (2) reproduced the gain derived from compatible emissions described by equation (1). The agreement between the two approaches for estimating the gain at 2100 and 2300 was within 2%, indicating the linear approximations used to derived equation (2) [e.g., *Gregory et al.*, 2009] were mostly reasonable. Then, we individually allowed α, β_O, β_L, γ_O, and γ_L terms to change to 2300 values, while holding all of the other terms in the equation at 2100 values. This analysis confirmed that most of the increasing gain originated from increases in γ_O and γ_L, that γ_O was the single most important driver, and that a reduction in α and increases in β_O and β_L partially offset the changes in γ (Figure 4).

The climate-carbon feedback parameter γ_O evolved in a similar way over time when estimated using either (1) the fully coupled and no CO_2 forcing simulations or (2) the fully coupled and no anthropogenic forcing

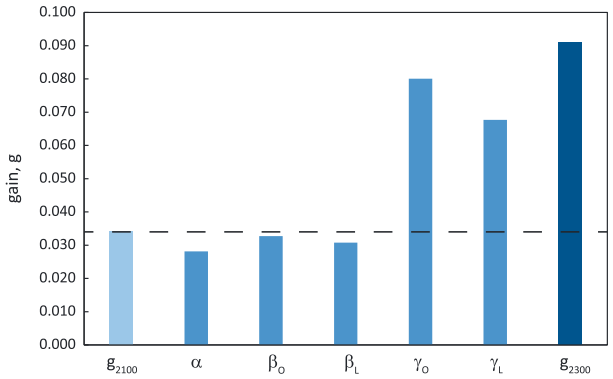

Figure 4. Contribution to increases in the gain between 2100 and 2300 as a function of changes in feedback parameters. The left bar shows the gain in the year 2100. The next five bars show the gain at 2300 if individual parameters are allowed to change to 2300 values, with all other parameters in equation (2) remaining at 2100 values. The final bar on the right shows the observed gain at 2300. Parameters with bars below the dashed line had the individual effect of reducing the gain, whereas parameters above the line caused it to increase. This figure illustrates that most of the increase in the gain between 2100 and 2300 was driven by the increasing magnitude of γ_O and γ_L and that changes in α, β_O, and β_L had an opposing effect.

simulations (Figure 5). Parameter γ_O had a larger magnitude (was more negative) after about year 2150 when estimated from the difference between the no CO_2 forcing and no anthropogenic forcing simulations. The larger magnitude γ_O computed from this difference (representing γ_O derived from non-CO_2 anthropogenic climate change) was likely a consequence of a different temporal trajectory of surface air temperature and ocean heating for non-CO_2 forcing agents. Specifically, more than 75% of the final global mean surface air temperature change (Figure 1) and more than 40% of the cumulative ocean heat flux from non-CO_2 anthropogenic forcing occurred prior to 2100. By means of mechanisms described below (section 3.3), this enabled a more complete (and effective) impact of these forcing agents on ocean processes influencing ocean anthropogenic CO_2 inflow in subsequent centuries. In contrast, for the fully coupled simulation, only 50% of the total surface warming and 25% of the change in cumulative ocean heat content had occurred by 2100.

3.3. Driving Mechanisms of Changing Feedback

The increasing sensitivity of ocean carbon fluxes to climate after 2100 was a consequence of several interacting factors. Climate change induced a significant weakening of the Atlantic meridional overturning circulation (AMOC). More than half of the total decrease in AMOC occurred during the 22nd century, with AMOC finally stabilizing around 5 sverdrups (1 Sv equals $10^6\,m^3\,s^{-1}$) by 2300 (Figure 6a). The decreases in overturning had the effect of weakening anthropogenic carbon uptake by intermediate and deep waters of the North Atlantic, particularly during the 22nd and 23rd centuries (Figure 7). These results are consistent with reductions in high-latitude North Atlantic mixed layer depths and ocean productivity by 2100 as reported by *Moore et al.* [2013] and with long-term AMOC changes observed in other versions of CESM for the RCP8.5 scenario [*Meehl et al.*, 2012, 2013].

Concurrently, global ocean surface stratification continued to build after 2100 as a consequence of warming in tropics and subtropics and warming and freshening of surface waters toward the poles. Although global mean surface stratification leveled off during the final century (Figure 6b), it continued to increase in regions that had higher rates of carbon uptake including the Southern Ocean (data not shown). Ocean heat content also increased steadily through the end of the simulation, in parallel with increases in γ_O (Figure 6c). Ocean heat content may serve as a useful metric of the magnitude of climate change impacts on ocean carbon uptake because it integrates the influence of temperature changes on dissolved inorganic carbon solubility and transport of carbon to the ocean interior [*Goodwin and Lenton*, 2009]. A linear relationship between γ_O and ocean heat content was observed for different simulation pairs (Figure 8), in contrast with the nonlinear relationship observed between γ_O and global mean surface air temperature change for CESM1(BGC) (Figures 5c and 5d). The linearity of the relationship between γ_O and ocean heat content is consistent with ESM results reported by *Bopp et al.* [2013], showing that ocean heat content change can explain variations in dissolved O_2 for different Representative Concentration Pathways, as a consequence of its influence on solubility and interactions between warming-induced stratification and the biological pump [*Keeling and Garcia*, 2002; *Frolicher et al.*, 2009]. Plotted as a function of ocean heat content, γ_O from the CESM1(BGC) 1%/yr CO_2 increase experiment analyzed by *Arora et al.* [2013] had a

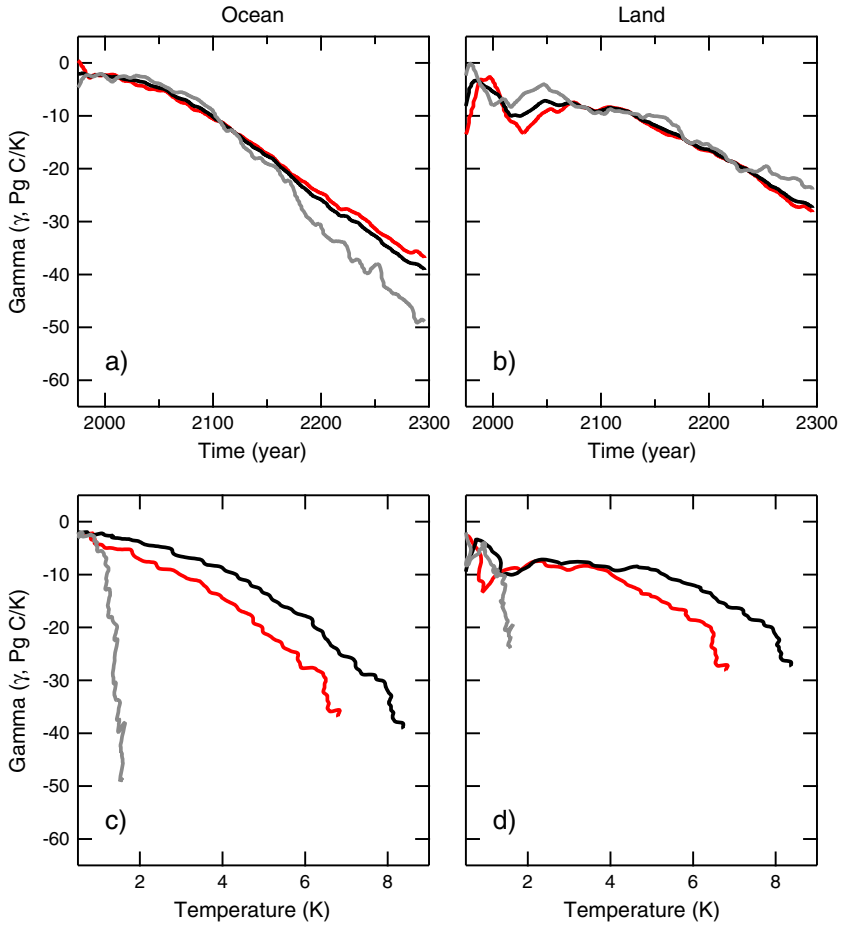

Figure 5. The sensitivity of carbon fluxes to climate change as a function of (a and b) time and (c and d) temperature. The ocean sensitivity (γ_O) is shown in Figures 5a and 5c, and the land sensitivity (γ_L) is shown in Figures 5b and 5d. Parameter γ computed from the fully coupled and no anthropogenic forcing simulations is shown in red, between the fully coupled and the no CO_2 forcing simulation in blue, and between the no CO_2 and no anthropogenic forcing simulations in gray.

similar but slightly steeper slope than the estimate derived here from the fully coupled and no CO_2 forcing simulations (Figure 8).

On land, net primary production in the tropics increased at a faster rate during the latter half of the 21st century in the fully coupled run than in the other two simulations (Figure 9a). This response was a consequence of increasing soil moisture availability from climate change enhancing gross primary production, particularly in Africa and Asia. After approximately 2150, net primary production decreased in the fully coupled simulation as a consequence of increasing maintenance respiration costs from higher surface air temperatures. In parallel, heterotrophic respiration rates were higher as a consequence of warmer temperatures and higher levels of soil moisture. As a result, the global land biosphere was a net source during the 23rd century in the fully coupled simulation (Figure 2b) but a sink in the other two simulations. Carbon losses induced from climate change were largest in areas dominated by forests (Figures 7e and 7f). In the tropics, climate-induced carbon losses were considerably higher in forests of Central and South America than in Africa or Asia, and the magnitude of the climate impact increased considerably from 2100 to 2300.

At midlatitude and high latitude (poleward of 40°N and 40°S), climate change in the fully coupled simulation led to higher rates of net primary production at all times (Figure 9b). In these regions, extension of the growing seasons and higher moisture availability more than offset the negative influence of increasing maintenance respiration costs. Similar to the tropics, however, heterotrophic respiration increased more in

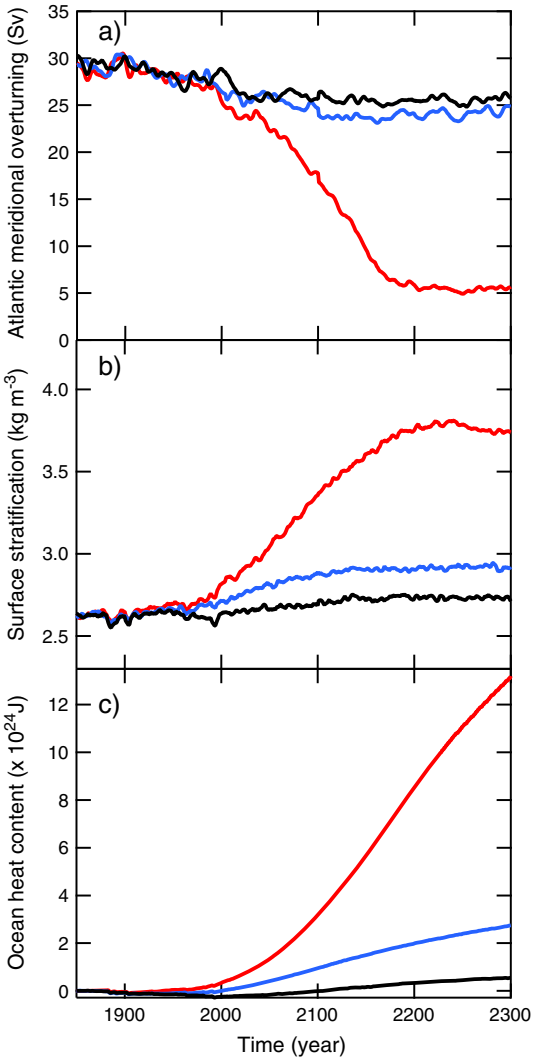

Figure 6. (a) Atlantic meridional overturning circulation (AMOC) defined for the region between 30°N and 50°N and 500 m to 2000 m in units of sverdrups (1 Sv = 10^6 m^3 s^{-1}), (b) global mean surface stratification defined as the density difference between 500 m and the surface layer in units of kg m^{-3}, and (c) difference in ocean heat content from the beginning of each simulation in units of joules integrated between 0 and 2000 m. The red lines denote the fully coupled simulation, the blue lines denote the no CO_2 forcing simulation, and the black lines denote the no anthropogenic forcing simulation.

response to climate change than net primary production, causing a net release of carbon in the fully coupled simulation from many boreal forest ecosystems.

4. Discussion

4.1. Increasing Relative Contribution of the Ocean to the Climate-Carbon Feedback

Our results are consistent with previous studies showing that the gain of the climate-carbon feedback increases as the Earth system is exposed to progressively higher levels of warming [*Friedlingstein et al.*, 2006; *Arora et al.*, 2013]. An unexpected outcome in the current study was the shift in the relative importance of ocean and land processes over time to the increasing gain. At first, γ_O had a smaller magnitude than γ_L. By 2100, however, the two terms were of similar size, and in subsequent centuries, the magnitude of γ_O exceeded γ_L. Several processes on land and in the oceans contributed to the increasing relative contribution over time of γ_O to the climate-carbon feedback in CESM1(BGC).

Within the oceans, the steady increase in heat content through the end of the fully coupled simulation (Figure 6c) influenced the ocean carbon cycle by means of at least three separate pathways. First, the continued ocean warming provided a driving gradient (through gas exchange) for temperature-driven dissolved inorganic carbon (DIC) solubility losses. Using a linear model to assess drivers of DIC changes, *Schwinger et al.* [2014] shows that this is a dominant mechanism contributing to ocean carbon losses from surface layers in CMIP5 models. Second, although the surface mixed layer adjusts relatively quickly to changes in atmospheric CO_2 levels (Figures 1a and 6b), ocean carbon uptake also is highly sensitive to mixing and transport processes that couple the mixed layer with intermediate and deep waters [*Primeau*, 2005; *Khatiwala et al.*, 2009]. Heat flow into these regions, potentially influencing diapycnal and isopycnal mixing as well as subduction, continued in CESM1(BGC) well after the mean global ocean surface density gradients had adjusted to a stabilization of atmospheric greenhouse gas levels (and as global mean surface air temperatures approached a new steady state). Finally, many ocean circulation systems that are important for carbon uptake, including the Atlantic meridional overturning circulation, respond nonlinearly to anthropogenic forcing (Figure 6a) and weaken significantly only after a threshold of heat inputs has been passed [*Weaver et al.*, 2012].

Concurrently, several processes on land in CESM1(BGC) likely limited the response of γ_L on longer time scales. All three of the simulations analyzed here included transient land use change through the year 2100 [*P. J. Lawrence et al.*, 2012]. For land use scenarios with expanding cropland and pasture areas (as is the case for

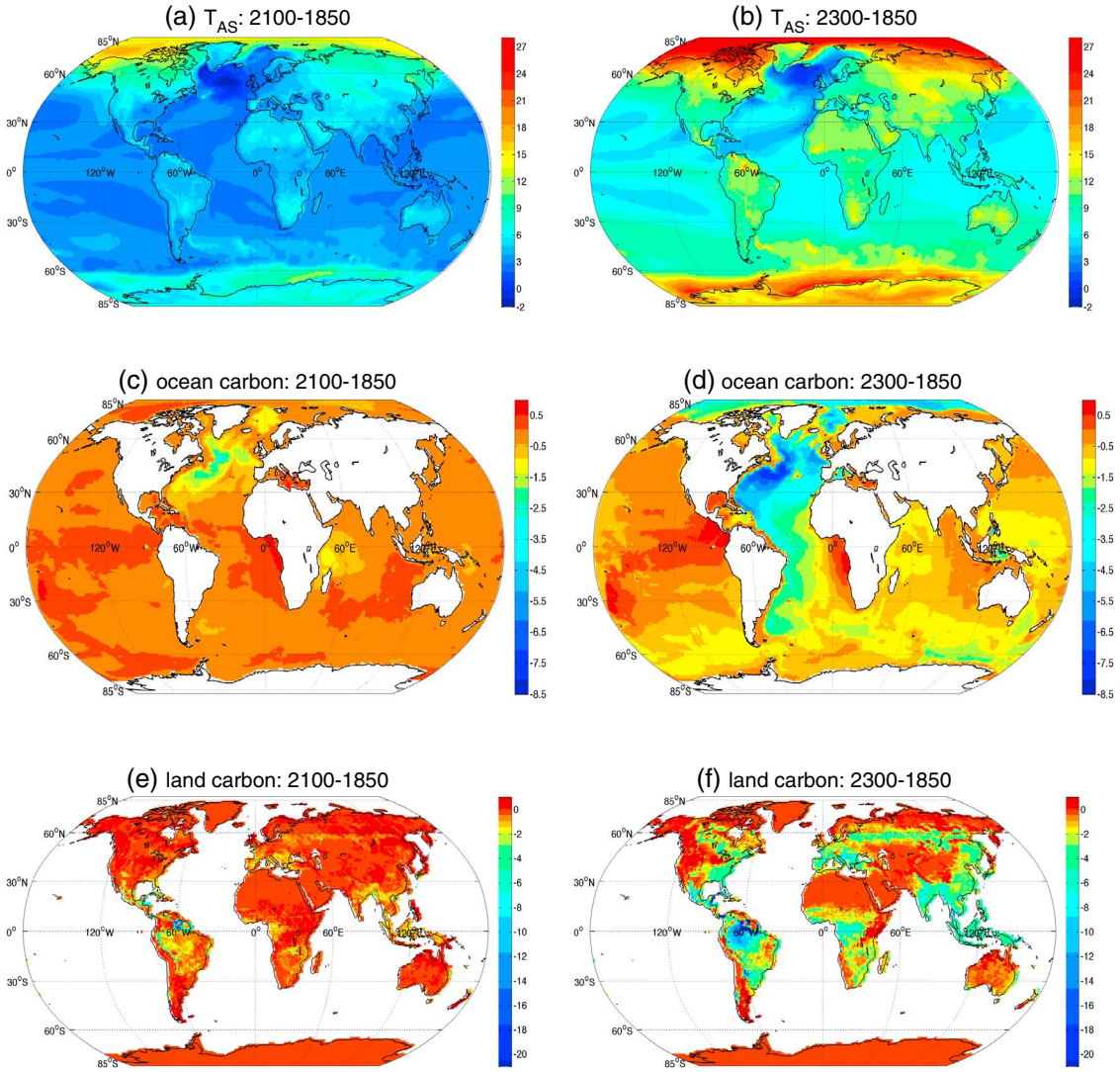

Figure 7. Surface air temperature changes (in units of kelvin) from the fully coupled simulation and climate change impacts on vertically integrated carbon stocks (kg C m^{-2}) at (a, c, and e) 2100 and (b, d, and f) 2300. For the ocean (Figures 7c and 7d) and land (Figures 7e and 7f), the difference in carbon stock between the fully coupled and the no anthropogenic forcing simulations is shown. Climate change often reduced land and ocean carbon storage, and so at most locations, there is a negative change in the inventory between the two simulations. By 2300, climate-induced reductions in ocean carbon were largest in the Atlantic and Arctic Oceans, whereas on land impacts were largest in tropical forests of Central and South America.

the RCP8.5 scenario), the loss of forest and soil organic matter carbon reservoirs likely reduced the magnitude of β_L and γ_L parameters [e.g., *Gitz and Ciais*, 2003]. For example, forest dieback in response to warming is moot if the area has already been converted to pasture. In addition, a lack of an explicit representation of permafrost processes and vegetation dynamics in these simulations limited carbon cycle responses to climate change. Although soil carbon pools in CESM1(BGC) are known to have a low bias [*Todd-Brown et al.*, 2013], whether this induces a significant low bias with respect to the response of the soil organic matter pool to temperature increases requires further evaluation of model turnover times with radiocarbon observations and other constraints.

An important next step is to conduct new simulations to quantify the influence of land use change on the carbon cycle feedbacks. In addition, improved representation of permafrost in a more recent version of the Community Land Model (CLM4.5) [*Koven et al.*, 2015] is expected to considerably increase carbon losses from the terrestrial biosphere in future coupled runs with CESM. Climate-induced permafrost carbon losses from CLM4.5 forced directly with a CESM RCP8.5 climate time series ranged between 66 and 207 Pg C by 2300 [*Koven et al.*, 2015]. Thus, including permafrost processes in a coupled simulation may lead to similar

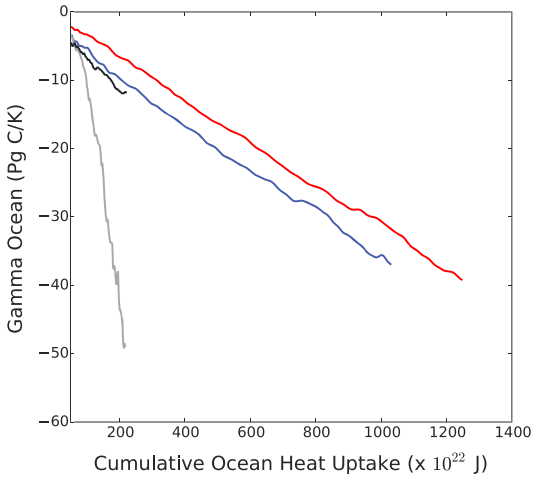

Figure 8. Parameter γ_O as a function of ocean heat content. Parameter γ_O and ocean heat uptake computed from difference between the fully coupled and no anthropogenic forcing simulations is shown in red, between the fully coupled and the no CO_2 forcing simulation in blue, and between the no CO_2 and no anthropogenic forcing simulations in gray. Parameter γ_O versus ocean heat uptake for CESM1(BGC) from the CMIP5 1%/yr CO_2 increase experiment analyzed by *Arora et al.* [2013] is overlain in black. For the CMIP5 simulations, we computed γ_O from the fully coupled and biogeochemistry coupled simulations.

contributions of land and ocean processes to climate-induced changes in carbon inventories. This approximate balance is still considerably different from the IPCC Fifth Assessment Working Group 1 consensus that γ_L is many times larger than γ_O, and as described below, is likely a consequence of several factors related to experiment design and simulation length.

4.2. Comparison of Climate-Carbon Feedback Parameters Among Different Studies

Comparison of ESMs contributing simulations to C4MIP (circa 2005) and CMIP5 (circa 2012) shows that the magnitude of the multimodel mean γ_O decreased more than threefold between the two studies, from -31 ± 16 to -8 ± 13 (1 SD) Pg C K^{-1}, with the CESM1-BGC result falling in the lower part of the range (-2.4 Pg C K^{-1}) [*Arora et al.*, 2013]. Parameter γ_L also decreased in magnitude, but by a smaller amount, from -78 ± 46 to -58 ± 29 (1 SD) Pg C K^{-1} and again with the CESM1-BGC value of -21 Pg C K^{-1} well below the multimodel mean. Drawing from these studies, the IPCC Fifth Assessment Report states that γ_O is typically 4–5 times smaller than γ_L [*Ciais et al.*, 2013]. Recent work by *Zickfeld et al.* [2011] and *Schwinger et al.* [2014] identify two primary causes for the large decrease in the reported magnitude of γ_O between C4MIP and CMIP5 related to nonlinear carbon cycle behavior within ESMs. *Zickfeld et al.* [2011] describes how γ inferred from a prescribed atmospheric CO_2 concentration scenario (i.e., CMIP5) may be lower than that inferred from a CO_2 emission scenario (C4MIP) because of the difficulty in estimating β, which tends to saturate as a function of increasing atmospheric CO_2. Thus, the *Friedlingstein et al.* [2006] study yields a set of γ values that are higher than what would be derived for the same set of models from a parallel analysis in which atmospheric CO_2 mole fractions were prescribed.

A parallel mechanism involves differences in the simulations used to compute γ between C4MIP and CMIP5. Here we follow the nomenclature from *Arora et al.* [2013] that defines a radiatively coupled simulation as one, in which increasing levels of atmospheric CO_2 influence radiative transfer within the atmosphere (and thus climate) but not the biogeochemistry. The complement is a biogeochemistry coupled run, in which increasing levels of atmospheric CO_2 influence the biogeochemistry but not radiative transfer. A fully coupled simulation is one, in which increasing levels of atmospheric CO_2 influence both radiative transfer and biogeochemistry—similar to the definition described above in the methods. In this context, when γ_O is estimated from fully coupled and biogeochemistry coupled simulations, it has a considerably larger magnitude than an estimate derived from a radiatively coupled simulation and a control [*Schwinger et al.*, 2014]. This is because for the former set of simulations, climate warming modifies the pathways for atmospheric anthropogenic CO_2 penetration into the ocean. For a radiatively coupled run, in which ocean biogeochemistry is exposed to atmospheric CO_2 held at preindustrial levels, the mechanism by which warming influences anthropogenic CO_2 inflow does not exist and so the primary influence of climate change is on ocean DIC solubility and changes in transport modifying the natural carbon cycle [*Schwinger et al.*, 2014]. The different climate sensitivity of these mechanisms is the primary reason why γ_O reported for CESM1(BGC) in *Arora et al.* [2013] (-2.4 Pg C K^{-1}) has a much smaller magnitude than the one we report here for the same model by 2100 (-10.1 Pg C K^{-1}). *Arora et al.* [2013] estimated γ for each model using the radiatively coupled and control simulations, whereas here we estimated it from simulations more analogous to the fully coupled and biogeochemistry coupled simulations. While the *Zickfeld et al.* [2011]

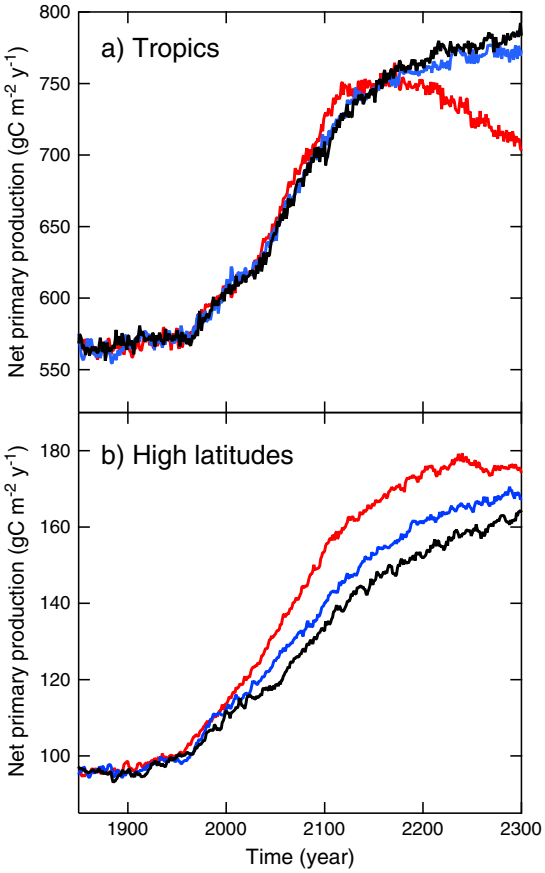

Figure 9. Terrestrial net primary production averaged in latitude bands over (a) tropical regions between 23°S and 23°N and (b) high latitudes north of 40° or south of 40°S. The red lines denote the fully coupled, the blue lines denote the no CO_2 forcing, and the black line denote the no anthropogenic forcing simulation.

analysis indicates that similar nonlinear interactions occur within land models, a systematic analysis of the land component of CMIP5 models has not yet been conducted.

Our results suggest that an additional factor contributes to differences in γ_O inferred from different studies—specifically the length of the simulation and thus cumulative amount of ocean heat uptake. For the CESM1(BGC) simulations analyzed here, the magnitude of γ_O was proportional to ocean heat content and more than tripled from 2100 to 2300 (Figure 5). CESM1(BGC) simulations contributed to the CMIP5 1%/yr CO_2 increase experiment (and analyzed by *Arora et al.* [2013]) exhibited this same proportionality but operate over a much smaller increment of change in ocean heat content (Figure 8). This suggests that γ_O estimates inferred from model intercomparison studies with longer simulations (and larger increases in ocean heat content) may have larger magnitudes. If this result holds for other models, then the C4MIP simulations from *Friedlingstein et al.* [2006] (that followed the Special Report on Emissions Scenarios A2 emission scenario for 250 years) would be expected to have larger changes in ocean heat content and γ_O values than the 140 year CMIP5 simulations analyzed by *Arora et al.* [2013]. Considering just CESM1(BGC), the change in ocean heat content at the end of the CMIP5 1%/yr CO_2 increase experiment was equivalent to the heat added up to the year 2080 for the RCP8.5 fully coupled simulation analyzed here. This corresponded to a point in time when ocean carbon fluxes were just beginning to visibly diverge among the different simulations shown in Figure 1. The increasing magnitude of γ through time observed here for CESM1(BGC) contrasts with an earlier analysis with the HadCM3LC model suggesting that γ was relatively constant [*Gregory et al.*, 2009]. Further research is needed to assess whether a relationship between γ_O and ocean heat content exists for other ESMs.

These findings and other recently published analyses [*Zickfeld et al.*, 2011; *Schwinger et al.*, 2014] suggest that several steps may be required to enable a systematic comparison of feedback parameters between C4MIP, CMIP5, and CMIP6. First, the use of fully coupled and biogeochemically coupled simulations may have advantages because of the sensitivity of this set to climate impacts on anthropogenic CO_2 inflow in the oceans [*Schwinger et al.*, 2014]. To enable backward compatibility, this will require recomputing feedback parameters and the gain from the CMIP5 models. Other adjustments for the influence of varying atmospheric CO_2 levels in fully coupled and biogeochemically coupled simulations on γ from C4MIP [*Gregory et al.*, 2009; *Zickfeld et al.*, 2011] may be possible and deserve exploration. Second, the continued use of standard simulation protocols (i.e., the 1% per increase to 4 × preindustrial CO_2) is critical to remove the influence of time- and scenario-dependent impacts on many parameters, including γ. Finally, because of the vastly different scale of physical climate system changes between these idealized simulations and the longer time horizons of many future CO_2 stabilization scenarios (e.g., Figure 8), more study is needed to understand how carbon cycle feedbacks are different in scenarios used extensively for mitigation and adaptation. Central for this latter challenge is the need for a new simulation protocol that enables

diagnosis of carbon cycle feedback parameters within a given scenario, taking into account carbon cycle interactions with land use change, nutrient loading, other greenhouse gases (including CH_4 and N_2O), and changes in atmospheric chemistry.

4.3. Implications for Climate Policy

Our experimental design provided some information relevant for the design of climate policy to avoid dangerous interference with the climate system, even though the RCP8.5 scenario analyzed here had rapid and sustained growth of fossil fuel emissions. Specifically, these simulations allowed us to isolate warming from CO_2 and non-CO_2 anthropogenic emissions. By the end of the 20th century, non-CO_2 atmospheric forcing yielded 0.5 K of warming. The contribution of this forcing increased to 1.3 K by 2100 and 1.6 K by 2300, with most of the warming occurring earlier in time than for warming originating from atmospheric CO_2 changes (Figure 1b). For a 2°C stabilization scenario, additional warming of a few tenths of a degree would be expected from the direct effect of atmospheric CO_2 on leaf stomatal conductance and other aspects of the land surface energy balance, although this could be modified by changes in land use. The relatively large magnitude of these temperature changes, relative to a possible 2°C threshold, illustrates why large investments in mitigation of non-CO_2 anthropogenic forcing agents are needed in parallel with requirements for CO_2 emission abatement [*Ramanathan and Feng*, 2008; *Shindell et al.*, 2012].

For the historical and RCP8.5 scenario, N_2O increases from 273 ppb in 1765 to 320 ppb by 2005 and to almost 500 ppb by 2100 [*Meinshausen et al.*, 2011]. Through 2050, *Davidson* [2012] shows that RCP8.5 scenario used by the IPCC is consistent with other projected trends in population, caloric intake, and meat consumption. Even with considerable modification of diet and improvements in agricultural and industrial efficiency, stabilization of N_2O levels below 350 ppb appears unlikely, and the representation of N_2O changes in lower radiative forcing RCPs, such as RCP3PD, may be overly optimistic.

In parallel, CH_4 levels increased in the historical and RCP8.5 scenario from 722 ppb in 1765 to 1755 ppb by 2005 and to over 3500 ppb by 2100. Although these are large projected changes in atmospheric CH_4 relative to recent changes, observations show that CH_4 is now increasing after a decadal hiatus [*Nisbet et al.*, 2014], partly from new oil and natural gas extraction technologies that have been shown to generate high levels of fugitive emissions [*Petron et al.*, 2014]. Further challenges in stabilizing N_2O and CH_4 levels are likely to originate from positive climate-ecosystem feedbacks, including biological responses to the intensification of the hydrological cycle on land and increases in ocean stratification that contribute to declining ocean oxygen concentrations and the expansion of oxygen minimum zones [*Stramma et al.*, 2008, 2010; *Bopp et al.*, 2013]. Important next steps are to integrate prognostic N_2O and CH_4 into CESM and to separate feedbacks to warming from individual greenhouse gases and aerosol processes.

5. Conclusions

Analysis of transient simulations to 2300 with CESM1(BGC) demonstrates that it is possible to assess quantitatively carbon cycle feedback processes for a Representative Concentration Pathway that includes non-CO_2 anthropogenic forcing agents. Ocean and land γ evolved similarly over time when exposed to climate change induced solely from CO_2 or from CO_2 and other anthropogenic atmospheric forcing agents. The ocean contribution to the climate-carbon feedback increased considerably over time for the RCP8.5 scenario and exceeded contributions from land after 2100. The strengthening of ocean climate-carbon feedback was consistent with the influence of ocean heat uptake on physical transport pathways for anthropogenic CO_2 inflow and temperature-dependent changes in the solubility of dissolved inorganic carbon. This is the first set of simulations, that we are aware of, that shows a reversal of the relative importance of ocean and land processes to the global climate-carbon feedback. Land use change likely reduced the sensitivity of terrestrial ecosystems to climate change by replacing forests with pastures and croplands, although further simulations are needed to isolate the magnitude of these effects. Regional reductions in carbon inventories from climate change were greatest in tropical forests in Central and South America and throughout the North Atlantic Ocean.

Our experimental design also allowed us to assess the amount of warming induced by forcing agents other than CO_2 as well as the sensitivity of ocean and land carbon cycle processes to this warming. Our analysis

suggests that improved representation of non-CO_2 forcing and feedback processes in ESMs is crucial for reducing uncertainties related to low-emission scenarios such as those designed to limit dangerous interference with the climate system. Important next steps include further assessment of land use change processes on evolution of climate-carbon feedbacks and integration of permafrost, CH_4, and N_2O processes within fully coupled CESM simulations.

Acknowledgments

We are grateful for support from the U.S. Department of Energy Office of Science and the National Science Foundation (NSF). J.T.R. and F.H. received support from the Regional and Global Climate Modeling Program in the Climate and Environmental Sciences Division of the Biological and Environmental Research (BER) Program in the U.S. Department of Energy Office of Science. J.T.R., K.L., E.M., W.F., J.K.M., S.C.D., and N.N.M. received funding from the NSF project "Collaborative Research: Improved Regional and Decadal Predictions of the Carbon Cycle" (AGS-1048827, AGS-1021776, and AGS-1048890). The Community Earth System Modeling project receives support from both NSF and BER. Computing resources were provided by the Climate Simulation Laboratory at NCAR's Computational and Information Systems Laboratory, sponsored by NSF and other agencies. The CESM1(BGC) simulation output analyzed here for the RCP/ECP8.5 scenario is available upon request. Please contact the authors for ftp access. The CESM1(BGC) simulations for the CMIP5 1%/yr CO_2 increase experiments are available on the Earth System Grid Federation (http://pcmdi9.llnl.gov/esgf-web-fe/). We thank C. Jones and an anonymous reviewer for their valuable suggestions during the review process.

References

Arora, V. K., et al. (2013), Carbon-concentration and carbon-climate feedbacks in CMIP5 Earth system models, *J. Clim.*, *26*(15), 5289–5314, doi:10.1175/jcli-d-12-00494.1.

Betts, R. A., P. M. Cox, M. Collins, P. P. Harris, C. Huntingford, and C. D. Jones (2004), The role of ecosystem-atmosphere interactions in simulated Amazonian precipitation decrease and forest dieback under global climate warming, *Theor. Appl. Climatol.*, *78*(1–3), 157–175, doi:10.1007/s00704-004-0050-y.

Bopp, L., et al. (2013), Multiple stressors of ocean ecosystems in the 21st century: Projections with CMIP5 models, *Biogeosciences*, *10*(10), 6225–6245, doi:10.5194/bg-10-6225-2013.

Boucher, O., P. R. Halloran, E. J. Burke, M. Doutriaux-Boucher, C. D. Jones, J. Lowe, M. A. Ringer, E. Robertson, and P. Wu (2012), Reversibility in an Earth System model in response to CO_2 concentration changes, *Environ. Res. Lett.*, *7*(2), doi:10.1088/1748-9326/7/2/024013.

Ciais, P., et al. (2013), Carbon and other biogeochemical cycles, in *Climate Change 2013: The Physical Science Basis. Contribution of Working Group I to the Fifth Assessment Report of the Intergovernmental Panel on Climate Change*, edited by T. F. Stocker et al., pp. 465–570, Cambridge Univ. Press, Cambridge, U. K., and New York, doi:10.1017/CBO9781107415324.014.

Collins, M., et al. (2013), Long-term climate change: Projections, commitments and irreversibility, in *Climate Change 2013: The Physical Science Basis. Contribution of Working Group I to the Fifth Assessment Report of the Intergovernmental Panel on Climate Change*, edited by T. F. Stocker et al., pp. 1029–1136, Cambridge Univ. Press, Cambridge, U. K., and New York, doi:10.1017/CBO9781107415324.024.

Cox, P. M., D. Pearson, B. B. Booth, P. Friedlingstein, C. Huntingford, C. D. Jones, and C. M. Luke (2013), Sensitivity of tropical carbon to climate change constrained by carbon dioxide variability, *Nature*, *494*(7437), 341–344, doi:10.1038/nature11882.

Danabasoglu, G., S. C. Bates, B. P. Briegleb, S. R. Jayne, M. Jochum, W. G. Large, S. Peacock, and S. G. Yeager (2012), The CCSM4 ocean component, *J. Clim.*, *25*(5), 1361–1389, doi:10.1175/jcli-d-11-00091.1.

Davidson, E. A. (2012), Representative Concentration Pathways and mitigation scenarios for nitrous oxide, *Environ. Res. Lett.*, *7*(2), doi:10.1088/1748-9326/7/2/024005.

Davidson, E. A., et al. (2012), The Amazon basin in transition, *Nature*, *481*(7381), 321–328, doi:10.1038/nature10717.

Field, C. B., et al. (2014), Technical summary, in *Climate Change 2014: Impacts, Adaptation, and Vulnerability. Part A: Global and Sectoral Aspects. Contribution of Working Group II to the Fifth Assessment Report of the Intergovernmental Panel on Climate Change*, edited by C. B. Field et al., Cambridge Univ. Press, Cambridge, U. K., and New York.

Friedlingstein, P., et al. (2006), Climate-carbon cycle feedback analysis: Results from the (CMIP)-M-4 model intercomparison, *J. Clim.*, *19*(14), 3337–3353, doi:10.1175/jcli3800.1.

Friedlingstein, P., et al. (2014), Persistent growth of CO_2 emissions and implications for reaching climate targets, *Nat. Geosci.*, *7*(10), 709–715, doi:10.1038/ngeo2248.

Froelicher, T. L., and F. Joos (2010), Reversible and irreversible impacts of greenhouse gas emissions in multi-century projections with the NCAR global coupled carbon cycle-climate model, *Clim. Dyn.*, *35*(7–8), 1439–1459, doi:10.1007/s00382-009-0727-0.

Frolicher, T. L., F. Joos, G. K. Plattner, M. Steinacher, and S. C. Doney (2009), Natural variability and anthropogenic trends in oceanic oxygen in a coupled carbon cycle-climate model ensemble, *Global Biogeochem. Cycles*, *23*, GB1003, doi:10.1029/2008GB003316.

Gent, P. R., et al. (2011), The Community Climate System Model version 4, *J. Clim.*, *24*(19), 4973–4991, doi:10.1175/2011jcli4083.1.

Gillett, N. P., V. K. Arora, D. Matthews, and M. R. Allen (2013), Constraining the ratio of global warming to cumulative CO_2 emissions using CMIP5 simulations, *J. Clim.*, *26*(18), 6844–6858, doi:10.1175/jcli-d-12-00476.1.

Gitz, V., and P. Ciais (2003), Amplifying effects of land-use change on future atmospheric CO_2 levels, *Global Biogeochem. Cycles*, *17*(1), 1024, doi:10.1029/2002GB001963.

Gloor, M., J. L. Sarmiento, and N. Gruber (2010), What can be learned about carbon cycle climate feedbacks from the CO_2 airborne fraction?, *Atmos. Chem. Phys.*, *10*(16), 7739–7751, doi:10.5194/acp-10-7739-2010.

Goodwin, P., and T. M. Lenton (2009), Quantifying the feedback between ocean heating and CO_2 solubility as an equivalent carbon emission, *Geophys. Res. Lett.*, *36*, L15609, doi:10.1029/2009GL039247.

Gregory, J. M., C. D. Jones, P. Cadule, and P. Friedlingstein (2009), Quantifying carbon cycle feedbacks, *J. Clim.*, *22*(19), 5232–5250, doi:10.1175/2009jcli2949.1.

Hansen, J., et al. (2005), Earth's energy imbalance: Confirmation and implications, *Science*, *308*(5727), 1431–1435, doi:10.1126/science.1110252.

Hansen, J., et al. (2013), Assessing "Dangerous climate change": Required reduction of carbon emissions to protect young people, future generations and nature, *Plos One*, *8*(12), e81648, doi:10.1371/journal.pone.0081648.

Hurrell, J. W., et al. (2013), The Community Earth System Model: A framework for collaborative research, *Bull. Am. Meteorol. Soc.*, *94*(9), 1339–1360, doi:10.1175/bams-d-12-00121.1.

Hurtt, G. C., et al. (2011), Harmonization of land-use scenarios for the period 1500–2100: 600 years of global gridded annual land-use transitions, wood harvest, and resulting secondary lands, *Clim. Change*, *109*(1–2), 117–161, doi:10.1007/s10584-011-0153-2.

Jones, C., et al. (2013), Twenty-first-century compatible CO_2 emissions and airborne fraction simulated by CMIP5 Earth system models under four Representative Concentration Pathways, *J. Clim.*, *26*(13), 4398–4413, doi:10.1175/jcli-d-12-00554.1.

Keeling, R. F., and H. E. Garcia (2002), The change in oceanic O_2 inventory associated with recent global warming, *Proc. Natl. Acad. Sci. U.S.A.*, *99*(12), 7848–7853, doi:10.1073/pnas.122154899.

Keppel-Aleks, G., et al. (2013), Atmospheric carbon dioxide variability in the Community Earth System Model: Evaluation and transient dynamics during the twentieth and twenty-first centuries, *J. Clim.*, *26*(13), 4447–4475, doi:10.1175/jcli-d-12-00589.1.

Khatiwala, S., F. Primeau, and T. Hall (2009), Reconstruction of the history of anthropogenic CO_2 concentrations in the ocean, *Nature*, *462*(7271), 346–U110, doi:10.1038/nature08526.

Koven, C. D., D. M. Lawrence, and W. J. Riley (2015), Permafrost carbon-climate feedback is sensitive to deep soil carbon decomposability but not deep soil nitrogendynamics, *Proc. Natl. Acad. Sci. U.S.A.*, *112*, 3752–3757, doi:10.1073/pnas.1415123112.

Kuhlbrodt, T., S. Rahmstorf, K. Zickfeld, F. B. Vikebo, S. Sundby, M. Hofmann, P. M. Link, A. Bondeau, W. Cramer, and C. Jaeger (2009), An integrated assessment of changes in the thermohaline circulation, *Clim. Change*, *96*(4), 489–537, doi:10.1007/s10584-009-9561-y.

Lamarque, J. F., et al. (2010), Historical (1850–2000) gridded anthropogenic and biomass burning emissions of reactive gases and aerosols: Methodology and application, *Atmos. Chem. Phys.*, *10*(15), 7017–7039, doi:10.5194/acp-10-7017-2010.

Lawrence, D. M., K. W. Oleson, M. G. Flanner, C. G. Fletcher, P. J. Lawrence, S. Levis, S. C. Swenson, and G. B. Bonan (2012), The CCSM4 land simulation, 1850–2005: Assessment of surface climate and new capabilities, *J. Clim.*, *25*(7), 2240–2260, doi:10.1175/jcli-d-11-00103.1.

Lawrence, P. J., et al. (2012), Simulating the biogeochemical and biogeophysical Impacts of transient land cover change and wood harvest in the Community Climate System Model (CCSM4) from 1850 to 2100, *J. Clim.*, *25*(9), 3071–3095, doi:10.1175/jcli-d-11-00256.1.

Lindsay, K., G. B. Bonan, S. C. Doney, F. M. Hoffman, D. M. Lawrence, M. C. Long, N. Mahowald, J. K. Moore, J. T. Randerson, and P. E. Thornton (2014), Preindustrial control and 20th century carbon cycle experiments with the Earth system model CESM1(BGC), *J. Clim.*, doi:10.1175/JCLI-D-12-00565.1.

Long, M. C., K. Lindsay, S. Peacock, J. K. Moore, and S. C. Doney (2013), Twentieth-century oceanic carbon uptake and storage in CESM1(BGC), *J. Clim.*, *26*(18), 6775–6800, doi:10.1175/jcli-d-12-00184.1.

Matthews, H. D., N. P. Gillett, P. A. Stott, and K. Zickfeld (2009), The proportionality of global warming to cumulative carbon emissions, *Nature*, *459*(7248), 829–U823, doi:10.1038/nature08047.

Meehl, G. A., W. M. Washington, J. M. Arblaster, A. X. Hu, H. Y. Teng, J. E. Kay, A. Gettelman, D. M. Lawrence, B. M. Sanderson, and W. G. Strand (2013), Climate change projections in CESM1(CAM5) compared to CCSM4, *J. Clim.*, *26*(17), 6287–6308, doi:10.1175/jcli-d-12-00572.1.

Meehl, G. A., et al. (2012), Climate system response to external forcings and climate change projections in CCSM4, *J. Clim.*, *25*(11), 3661–3683, doi:10.1175/jcli-d-11-00240.1.

Meinshausen, M., et al. (2011), The RCP greenhouse gas concentrations and their extensions from 1765 to 2300, *Clim. Change*, *109*(1–2), 213–241, doi:10.1007/s10584-011-0156-z.

Moore, J. K., K. Lindsay, S. C. Doney, M. C. Long, and K. Misumi (2013), Marine ecosystem dynamics and biogeochemical cycling in the Community Earth System Model CESM1(BGC): Comparison of the 1990s with the 2090s under the RCP4.5 and RCP8.5 scenarios, *J. Clim.*, *26*(23), 9291–9312, doi:10.1175/jcli-d-12-00566.1.

Myhre, G., E. J. Highwood, K. P. Shine, and F. Stordal (1998), New estimates of radiative forcing due to well mixed greenhouse gases, *Geophys. Res. Lett.*, *25*(14), 2715–2718, doi:10.1029/98GL01908.

Neale, R. B., J. Richter, S. Park, P. H. Lauritzen, S. J. Vavrus, P. J. Rasch, and M. H. Zhang (2013), The mean climate of the Community Atmosphere Model (CAM4) in forced SST and fully coupled experiments, *J. Clim.*, *26*(14), 5150–5168, doi:10.1175/jcli-d-12-00236.1.

Nisbet, E. G., E. J. Dlugokencky, and P. Bousquet (2014), Methane on the rise—Again, *Science*, *343*(6170), 493–495, doi:10.1126/science.1247828.

Petron, G., et al. (2014), A new look at methane and nonmethane hydrocarbon emissions from oil and natural gas operations in the Colorado Denver-Julesburg Basin, *J. Geophys. Res. Atmos.*, *119*, 6836–6852, doi:10.1002/2013JD021272.

Plattner, G. K., et al. (2008), Long-term climate commitments projected with climate-carbon cycle models, *J. Clim.*, *21*(12), 2721–2751, doi:10.1175/2007jcli1905.1.

Primeau, F. (2005), Characterizing transport between the surface mixed layer and the ocean interior with a forward and adjoint global ocean transport model, *J. Phys. Oceanogr.*, *35*(4), 545–564, doi:10.1175/jpo2699.1.

Ramanathan, V., and Y. Feng (2008), On avoiding dangerous anthropogenic interference with the climate system: Formidable challenges ahead, *Proc. Natl. Acad. Sci. U.S.A.*, *105*(38), 14,245–14,250, doi:10.1073/pnas.0803838105.

Schwinger, J., et al. (2014), Nonlinearity of ocean carbon cycle feedbacks in CMIP5 Earth system models, *J. Clim.*, *27*(11), 3869–3888, doi:10.1175/jcli-d-13-00452.1.

Shindell, D., et al. (2012), Simultaneously mitigating near-term climate change and improving human health and food security, *Science*, *335*(6065), 183–189, doi:10.1126/science.1210026.

Solomon, S., G. K. Plattner, R. Knutti, and P. Friedlingstein (2009), Irreversible climate change due to carbon dioxide emissions, *Proc. Natl. Acad. Sci. U.S.A.*, *106*(6), 1704–1709, doi:10.1073/pnas.0812721106.

Stramma, L., G. C. Johnson, J. Sprintall, and V. Mohrholz (2008), Expanding oxygen-minimum zones in the tropical oceans, *Science*, *320*(5876), 655–658, doi:10.1126/science.1153847.

Stramma, L., S. Schmidtko, L. A. Levin, and G. C. Johnson (2010), Ocean oxygen minima expansions and their biological impacts, *Deep Sea Res., Part I*, *57*(4), 587–595, doi:10.1016/j.dsr.2010.01.005.

Tebaldi, C., and P. Friedlingstein (2013), Delayed detection of climate mitigation benefits due to climate inertia and variability, *Proc. Natl. Acad. Sci. U.S.A.*, *110*(43), 17,229–17,234, doi:10.1073/pnas.1300005110.

Todd-Brown, K. E. O., J. T. Randerson, W. M. Post, F. M. Hoffman, C. Tarnocai, E. A. G. Schuur, and S. D. Allison (2013), Causes of variation in soil carbon simulations from CMIP5 Earth system models and comparison with observations, *Biogeosciences*, *10*(3), 1717–1736, doi:10.5194/bg-10-1717-2013.

Todd-Brown, K. E. O., et al. (2014), Changes in soil organic carbon storage predicted by Earth system models during the 21st century, *Biogeosciences*, *11*(8), 2341–2356, doi:10.5194/bg-11-2341-2014.

Weaver, A. J., et al. (2012), Stability of the Atlantic meridional overturning circulation: A model intercomparison, *Geophys. Res. Lett.*, *39*, L20709, doi:10.1029/2012GL053763.

Wenzel, S., P. M. Cox, V. Eyring, and P. Friedlingstein (2014), Emergent constraints on climate-carbon cycle feedbacks in the CMIP5 Earth system models, *J. Geophys. Res. Biogeosci.*, *119*, 794–807, doi:10.1002/2013JG002591.

Zickfeld, K., M. Eby, H. D. Matthews, A. Schmittner, and A. J. Weaver (2011), Nonlinearity of carbon cycle feedbacks, *J. Clim.*, *24*(16), 4255–4275, doi:10.1175/2011jcli3898.1.

Zickfeld, K., M. Eby, and A. J. Weaver (2008), Carbon-cycle feedbacks of changes in the Atlantic meridional overturning circulation under future atmospheric CO_2, *Global Biogeochem. Cycles*, *22*, Gb3024, doi:10.1029/2007GB003118.

Zickfeld, K., et al. (2013), Long-term climate change commitment and reversibility: An EMIC intercomparison, *J. Clim.*, *26*(16), 5782–5809, doi:10.1175/jcli-d-12-00584.1.